Available online at www.sciencedirect.com
ScienceDirect
Theoretical and Applied Fracture Mechanics 47 (2007) 15–25
theoretical and applied fracture mechanics
www.elsevier.com/locate/tafmec

Further study on effect of concrete defense layer on evolution mechanism of stress-waves

Z.L. Wang *, Y.C. Li

Department of Modern Mechanics, University of Science and Technology of China, Anhui province, Hefei 230027, China

Available online 27 November 2006

Abstract

The *Taylor–Chen–Kuszmaul* model, which regards the dynamic fracture process of brittle materials as a continuous accrual of damage, has been successfully applied to simulate rock blast and concrete penetration. This paper employs the TCK damage model to numerical study on the effect of perforated concrete defense layer on evolution mechanism of blast-induced stress waves. The numerical results reveal that the tensile damage near free boundary should be noteworthy under a higher blast loading, and the peak values of hydrostatic pressure beneath an artificial cavity are largely reduced. The effects of cavity dimensions and position on wave evolution and reduction are detailedly explored. One empirical formula is proposed to relate the decay factor of peak hydrostatic pressure to the dimensions and relative position of cavity.

Keywords: Defense system; Blast loading; Rectangular cavity; Tensile damage; Attenuation; Empirical formula

1. Introduction

Concrete has been widely used for military and civil purposes over many years. A review of previous work reveals that many studies of concrete shelters from the early 1940s. However, most of this work ceased shortly after World War II and was not resumed until the 1960s. The resistance of concrete against dynamic loadings is of great interest to both the designers of defense structures and the developers of weapon systems [1–3].

Many findings have shown that short-duration high-magnitude blast loading conditions significantly influence defense structural response. It well known that blast loadings are quite different from the conventional loads. For Example, they are typically applied to structures at rates approximately 1000 times faster than earthquake-induced loadings [4]. Consequently, the analysis of shelters made of brittle concrete subjected to blast loading becomes a very complex issue.

Generally speaking, the blast waves would evolve into the propagation of stress-waves in certain medium. The waves can be diffracted when hitting obstacles such as cavity and crevice, and its stress intensity may be greatly reduced after these obstacles. This reduction course is often termed as attenuation of stress-waves [5,6].

New stress-wave migration approaches are in expectation because the attenuation of stress-waves

* Corresponding author. Fax: +86 551 3606459.
E-mail address: Geowzl@yahoo.com.cn (Z.L. Wang).

0167-8442/$ - see front matter © 2006 Elsevier Ltd. All rights reserved.
doi:10.1016/j.tafmec.2006.10.002

is an ongoing topic of interest in the design of concrete defense structures. A better understanding of structural details behavior under blast loadings is very important, and a strong interest exists in developing methods to insure superior protective performance. For this sake, some experimental tests related have been performed by the authors, and a series of field observations were conducted. Fig. 1 is the appearance of full-scale test, and Fig. 2 depicts the schematic of the experimental defense system conducted in this project. Fig. 3 shows the defense roof permeated by blasting cracks after testing. Detailed presentations of the full-scale tests were demonstrated in [7]. It is clear that a layered defense system consists of three layers: a soil cover layer, a protection layer and a support layer. Furthermore, the protection layer has two sub-layers: a projectile shelter layer and a stress distribution layer. The stress distribution layer is inbuilt with artificial cavity here, whose function is to redistribute the blast loading over a larger area. However, studies on the function of the stress distribution layer are

Fig. 1. Appearance of field test for defense structure.

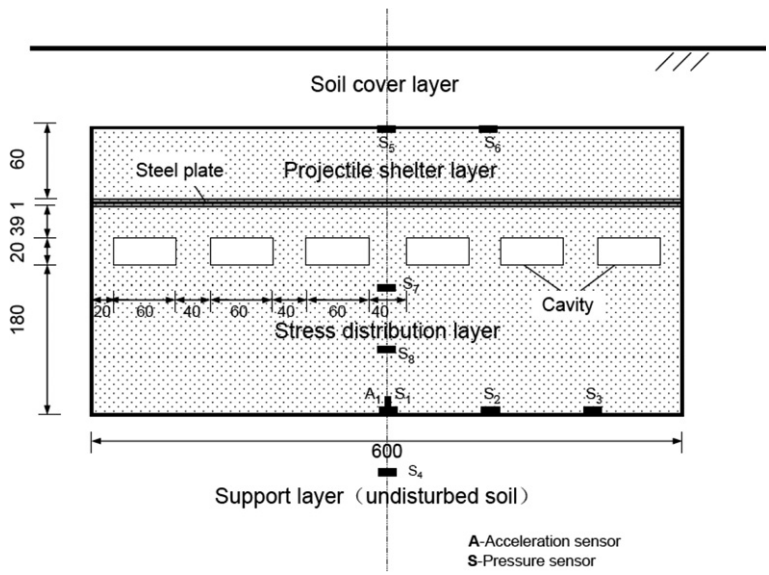

Fig. 2. Schematic of the defense structure for one field test.

Fig. 3. Roof of the protection layer in field test.

limited so far [7–9]. Besides, post-test observations show that spallation and even crater are formed at the top of cavities or near the non-transmission boundaries of defense system under a higher blast loading. The formation of the spallations is due mainly to dynamic fracture caused by the reflected tensile waves. Those phenomena ignored in the previous studies [7,9] will be paid more attention to in this work.

The remainder of this paper is organized as follows: In Section 2, the TCK continuum damage model [10,11] for brittle concrete is introduced and succinctly implemented into LS-DYNA [12]. The prerequisites for numerical analyses are given in Section 3, including the verification of the newly-implemented numerical tool. Section 4 numerically explores the effect of a single rectangular cavity on the attenuation of stress-waves, and one empirical formula is brought forward to relate the decay factor for peak P to the cavity parameters. At last, some conclusions and remarks are stated in Section 5.

The primary purpose of this paper is to investigate the dynamic responses of perforated concrete defense systems using the TCK damage model and provide references to the designers of intelligent protective shelters.

2. Description of TCK damage model

Concrete is typically brittle and non-homogeneous in composition. The basic assumption of the damage model is that the concrete is permeated by an array of randomly distributed cracks which grow and interact with one another under tensile loading. The damage is reflected in the degradation of the material stiffness following the equations derived in [13] for a random array of penny-shaped cracks in an isotropic elastic medium. The effective bulk modulus of the cracked solid is

$$\frac{\overline{K}}{K} = 1 - \frac{16}{9} f(\bar{v}) C_{\mathrm{d}} \tag{1}$$

where $f(\bar{v}) = (1-\bar{v}^2)/(1-2\bar{v})$, K and v are the original elastic constants (bulk modulus and Possion's ratio) for intact material, and barred quantities represent the corresponding degraded constants for the damaged material. C_{d} is the crack density parameter, which is assumed to be proportional to the product of N, the number of cracks of per unit volume, and r^3, the cube of the average crack dimension in a representative volume. Following the work in [14], N is expressed as a Weibull statistical distribution function activated by the bulk strain measure $\varepsilon_v = (\varepsilon_x + \varepsilon_{\mathrm{y}} + \varepsilon_z)/3$, according to

$$N = k(\varepsilon_v)^m \tag{2}$$

where k and m are material constants to be determined from strain-rate dependent tensile fracture stress data.

To extent the range of crack densities, an expression

$$\bar{v} = v \exp\left(-\frac{16}{9}\beta C_{\mathrm{d}}\right), \quad 0 \leqslant \beta \leqslant 1 \tag{3}$$

based on the percolation theory [15] was used for the equivalent Poisson's ratio $\bar{v}$. The value of β controls the unloading and reloading behaviors and relaxes the restriction of elastic unloading in the original model [16].

Based on kinetic energy consideration, an expression is derived [17] for the nominal fragment radius for dynamic fragmentation in a brittle material as:

$$r = \frac{1}{2}\left(\frac{\sqrt{20}K_{IC}}{\rho C\dot{\varepsilon}_{v\max}}\right)^{2/3} \tag{4}$$

In Eq. (4) ρ is the mass density, C is the uniaxial wave speed $\left(\sqrt{E/\rho}\right)$, $\dot{\varepsilon}_{v\max}$ is the maximum volumetric strain rate experienced by the representative volume element for the entire loading process, and K_{IC} is the fracture toughness of the material.

When bulk tension occurs in the material, the crack density parameter C_d can be calculated as:

$$C_d = \frac{5}{2}k(\varepsilon_v)^m\left(\frac{K_{IC}}{\rho C}\right)^2\dot{\varepsilon}_{v\max}^{-2} \tag{5}$$

From Eq. (1), the damage scalar can be calculated as follows:

$$D = \frac{16}{9}f_1(\bar{v})C_d \tag{6}$$

The degraded shear modulus $\overline{G}$ and Bulk modulus $\overline{K}$ are written as:

$$\begin{cases}\overline{G} = G(1-D)\\ \overline{K} = K(1-D)\end{cases} \tag{7}$$

Using Eq. (7), the elastic strain relations for stress are then adopted in $K-G$ form for bulk tension of concrete:

$$\Delta\sigma_{ij} = \overline{K}\Delta\varepsilon_{kk}\delta_{ij} + 2\overline{G}\Delta e_{ij} \tag{8}$$

where $\delta_{ij} = 0$ for $i \neq j$ and $\delta_{ij} = 1$ for $i = j$. $\Delta\sigma_{ij}$ and Δe_{ij} are increment for the stress tensor and the deviatoric strain tensor, respectively, and $\Delta\varepsilon_{kk}$ is the volumetric strain increment.

The plastic/kinematic algorithm used here for the response of concrete in compression is the usual elastic radial-return approach found in most nonlinear finite element codes [18].

The von Mises yield condition is expressed as:

$$\varphi = \tilde{\sigma}^2 - \sigma_y^2 \tag{9}$$

where $\tilde{\sigma} = \sqrt{\frac{3}{2}(s_{ij}-\omega_{ij})(s_{ij}-\omega_{ij})}$, σ_y denotes the yield stress which is assumed constant.

The center of the yield in deviatoric stress space is given by tensor $\boldsymbol{\omega}$ which has initial value of zero. The increment of $\boldsymbol{\omega}$ is given by:

$$\Delta\omega_{ij} = \frac{2}{3}E_p\dot{\varepsilon}_{ij}^p dt \tag{10}$$

where dt is the time step, E_p is the plastic hardening modulus, and the plastic strain ratio $\dot{\varepsilon}_{ij}^p$ is the difference between total and elastic strain (right superscript e) ratios:

$$\dot{\varepsilon}_{ij}^p = \dot{\varepsilon}_{ij} - \dot{\varepsilon}_{ij}^e \tag{11}$$

Table 1 gives the main concrete parameters for this concrete damage model [11].

3. Preconditions for numerical simulations

3.1. Equivalent blast loading

As indicated in Fig. 4, the planar charge in the field research program is adopted. Because the rise time of blast loading is very short and the overpressure decays exponentially after the peak value, an equivalent triangular pressure pulse (see Fig. 5) is used to approximate the blast loading [9,19,20]. In the present study, the peak value Q_{max} is taken as 120.0 MPa at time $t_{max} = 0.0$ μs (micro second) and then decreases linearly to zero at time $t_c = 100.0$ μs. It is in response to the display of pressure sensors S_5 and S_6 (see Fig. 2) and directly applied on the upper surface of the projectile shelter layer.

3.2. Implementation of the constitutive model

The hydrocode LS-DYNA from the *Livermore Software Technology Corporation* is used for the numerical analyses in this article. It can handle either two- or three- dimensional problems for explosion and high-speed impact [12,21].

Table 1
Material parameters for concrete

ρ (kg.m^{-3})	E (GPa)	v	σ_y (MPa)	k (m^{-3})	M	K_{IC} (MPa.m$^{-1/2}$)
2520.0	20.68	0.18	20.0	5.753e21	6.0	2.747

Fig. 4. Field assembly of blasting fuses for planar charge.

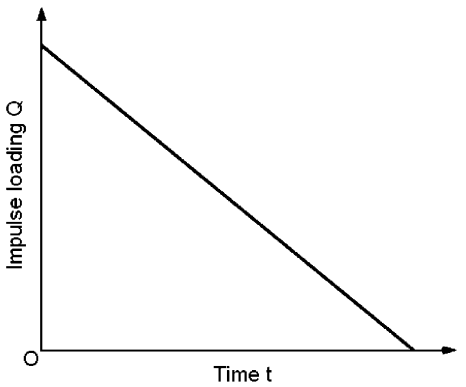

Fig. 5. Triangular impulse loading for explosion.

The TCK model described above has been implemented as a constitutive augmentation to the dynamic finite code LS-DYNA, and the detailed flowchart is illustrated in Fig. 6. The implementation follows general guidelines for such augmentation and employs the given interface subroutines. The augmentation is vectorized consistent with the basic LS-DYNA code, and incorporates damage as a history variable.

3.3. Verification of user define subroutine

This model was ever used in a study of blast induced damage in rock by Taylor et al. [10]. The single column of high explosive (Iregel 1175U) was bottom detonated. It was 2.5 m in height, 0.081 m in radius, and was centered at 3.75 m below the ground surface. The oil shale was assumed to be isotropic and homogenous material with pre-existing micro cracks. Included in [10] were the constitutive parameters for the rock and the explosive. Fig. 7 shows a comparison between the numerical predictions with the measured data of radial stress in place at a radial distance of 3.0 m and a depth of 2.5 m. It can be found that the developed user subroutine is capable of calculating the stress with good accuracy.

Fig. 2 shows the schematic drawing for one field experiment. A series of on-site observations were conducted. In numerical simulations, only the right-half domain is considered, and a total of 3636 quadrilateral elements are used, including 180 elements for steel plate. The steel plate is modeled with material Type 3 available in LS-DYNA. It is a bi-linear elastoplastic model. Table 2 lists the material parameters for the steel plate. The blast loading shown in Fig. 5 is applied upon the projectile shelter layer. A comparison between the measured with calculated wave forms of hydrostatic pressure in the place of sensor S_8 (see Fig. 2) is shown in Fig. 8. The sensor S_8 is at a depth of 1.25 m beneath the lower side of cavity. It can be seen that the numerical simulation of the peak value and waveform show a consistent comparison with the measured data. However, the tensile phenomenon is obvious in the curve tail for the numerical case. The reason is that the lower boundary of the calculation domain is regarded as a reflected one (i.e. non-transmission) in simulations. In fact, there exist soil layers beneath the defense system.

4. Attenuation effect of single cavity on stress-waves

In the field tests, multiple rectangular cavities were adopted (refer to Fig. 2). How about the effect of single cavity on attenuation of stress-waves? This section will investigate it based on the above verified numerical tool.

4.1. Definition of decay factor

To evaluate the attenuation extent of a stress-wave due to a cavity in a concrete defense system, a dimensionless variable, 'decay factor' DF, is defined as follows:

$$\mathrm{DF} = \frac{\sigma_0 - \sigma}{\sigma_0} \tag{12}$$

where σ_0 denotes the peak value of stress component, such as σ_x, τ_{xy}, and hydrostatic pressure P at a specified position without cavity in the defense layer, and σ is the peak value of the same component at the same position with a cavity in the

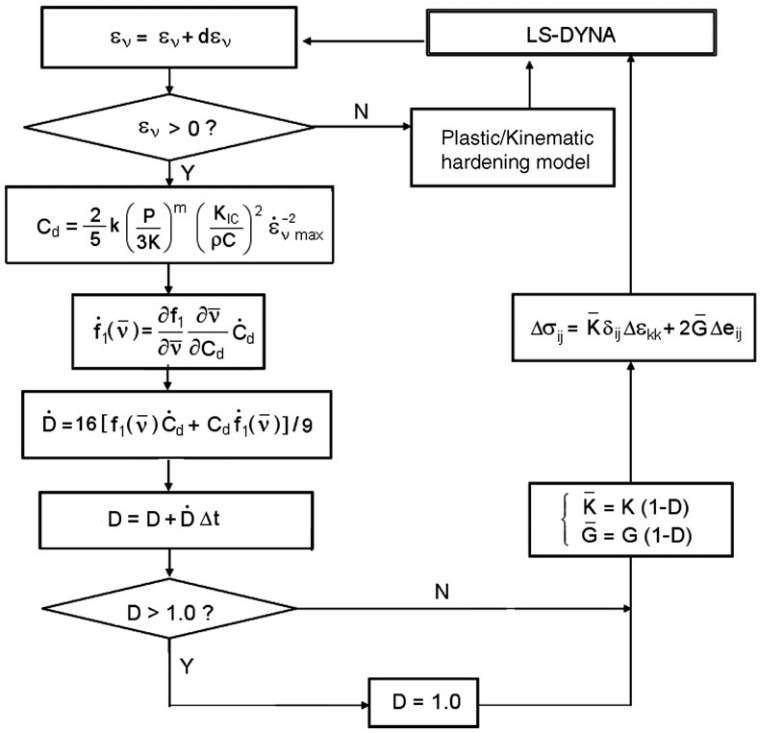

Fig. 6. Implementation flowchart for the TCK model.

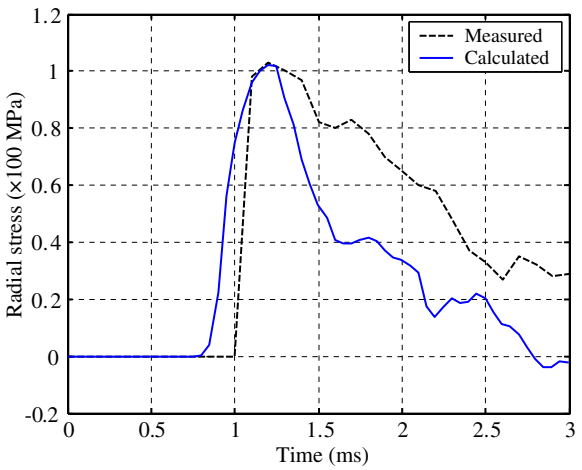

Fig. 7. Comparison between calculated and measured data for radial stress.

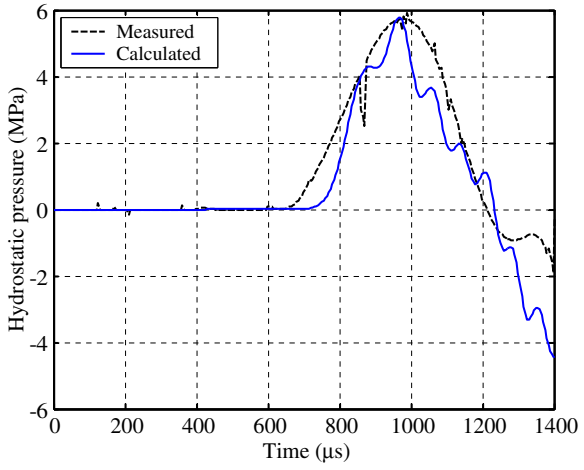

Fig. 8. Comparison between calculated and measured data for hydrostatic pressure.

Table 2
Material parameters for steel plate

ρ (kg m^{-3})	E (GPa)	v	σ_y (MPa)
7900.0	207.0	0.29	340.0

defense layer. Eq. (12) reveals that a larger DF would imply a better attenuation effect.

4.2. Computational domain with cavity

Fig. 9 shows a typical concrete defense layer embedded with a rectangular cavity. The computational domain for this plane strain model is taken as 600 cm × 300 cm (width × height). The embedded

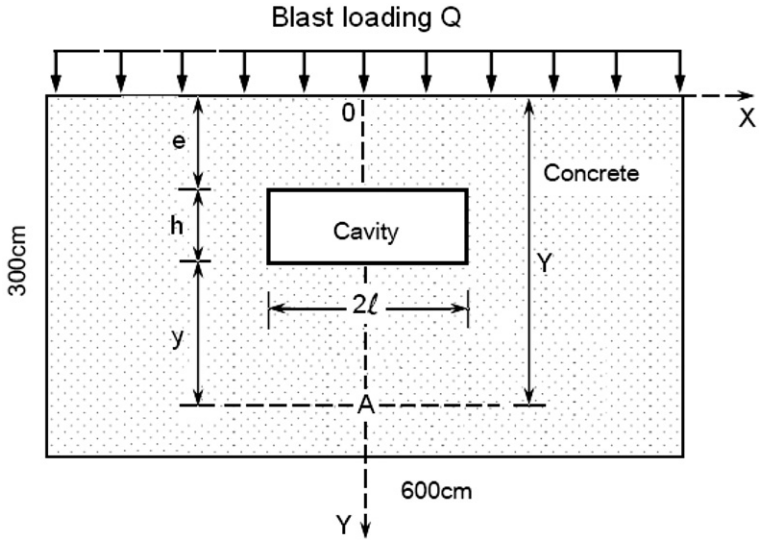

Fig. 9. Simulation of a perforated stress distribution layer.

cavity cross-section has the dimensions of $2l$ in length and h in width. Other dimensions are indicated in Fig. 9. Introducing the term relative distance y as the distance between point A and the lower side of the cavity, the dimension Y has the following relationship:

$$Y = y + e + h \tag{13}$$

A half domain is considered here owing to symmetry. As an example, the right-half domain shown in Fig. 9 has the following boundary conditions: traction boundary on the top, non-transmission boundaries on the right and lower sides, and symmetric boundary on the left side.

4.3. Analysis of cavity parameters on stress-waves

4.3.1. Effect of cavity length l

Five lengths are taken in the computations: 0.00, 0.30, 0.60, 0.90 and 1.20 m. Other geometrical parameters are fixed as $e = 0.6$ m and $h = 0.3$ m. Fig. 10 shows the effect of different lengths l on the attenuation of the peak P. For comparisons, the computations are also carried out based on the linear–elastic (L–E) model. The variations of peak P with relative distance y (refer to definition shown in Fig. 9) are shown in Fig. 10(a) for the L–E model and Fig. 10(b) for the TCK model. The results show that the peak P increases with relative distance y and decreases with increasing length l. It can also be seen that the elastoplastic properties of concrete plays a crucial role on the magnitude of peak P.

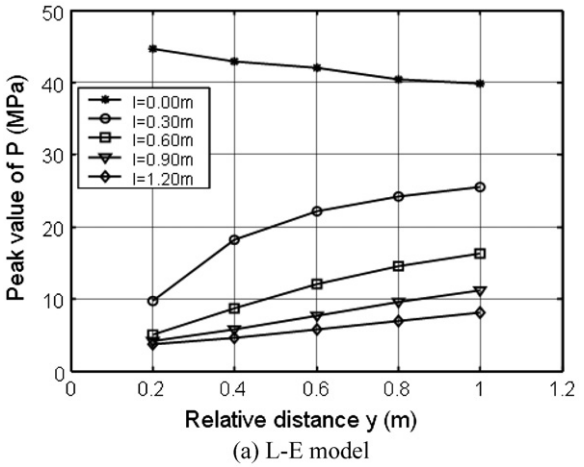

Fig. 10. Effect of different lengths l of cavity on peak hydrostatic pressure.

For instance, when $l = 0.30$ m and $y = 0.80$ m, the peak P is 24.25 MPa for the L–E model and only 9.29 MPa for the TCK model. The corresponding relationship between DF for the peak P and relative distance y is shown in Fig. 11. It can be established that DF decreases with increasing y and increases with cavity length for the same y.

Fig. 12 shows the hydrostatic pressure contours for the cases with or without cavity. A higher tensile stress region is observed above the cavity, and the maximum tension is about 12.1 MPa at $t = 347.8$ μs. The peak P beneath the cavity is evidently lower and even approaches zero. In addition, the reflected tensile waves can also be found near the left and right boundaries. As for the non-cavity case shown in Fig. 12(b), it is evident that the continuity of wave front is hardly interrupted and the tensile stress zones only rise at the side boundaries of the domain.

Assuming the duration of blast loading proportional to its peak value, Fig. 13 compares the simulated tensile damage for different situations. Clearly, more serious tensile damage above the cavity and near the boundaries can be noticed with the increment of blast loading. It is because the reflected ten-

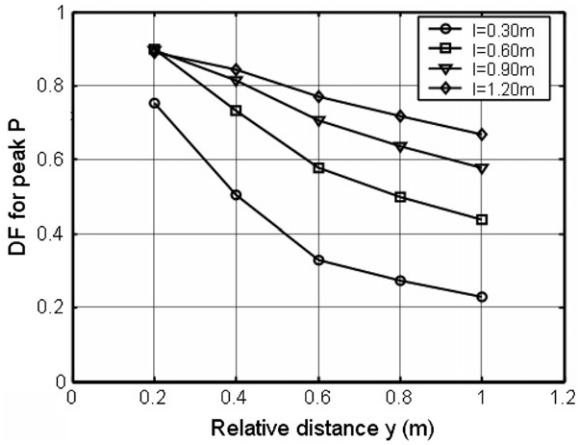

Fig. 11. Variation of decay factors for peak P with different lengths of cavity for TCK model.

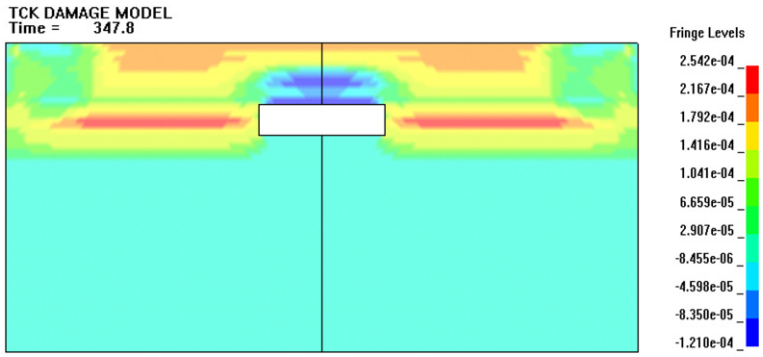

(a) With cavity (l=60cm, h=30cm and e=60cm)

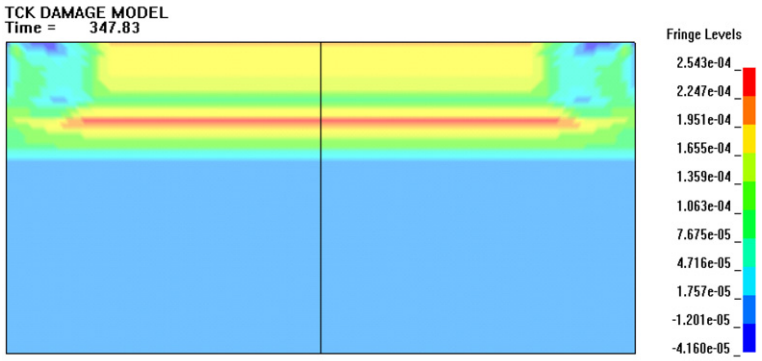

(b) Without cavity

Fig. 12. Contours of hydrostatic pressure for cases with and without cavity at the same time (Unit: Mbar. 1Mbar = 10^5 MPa).

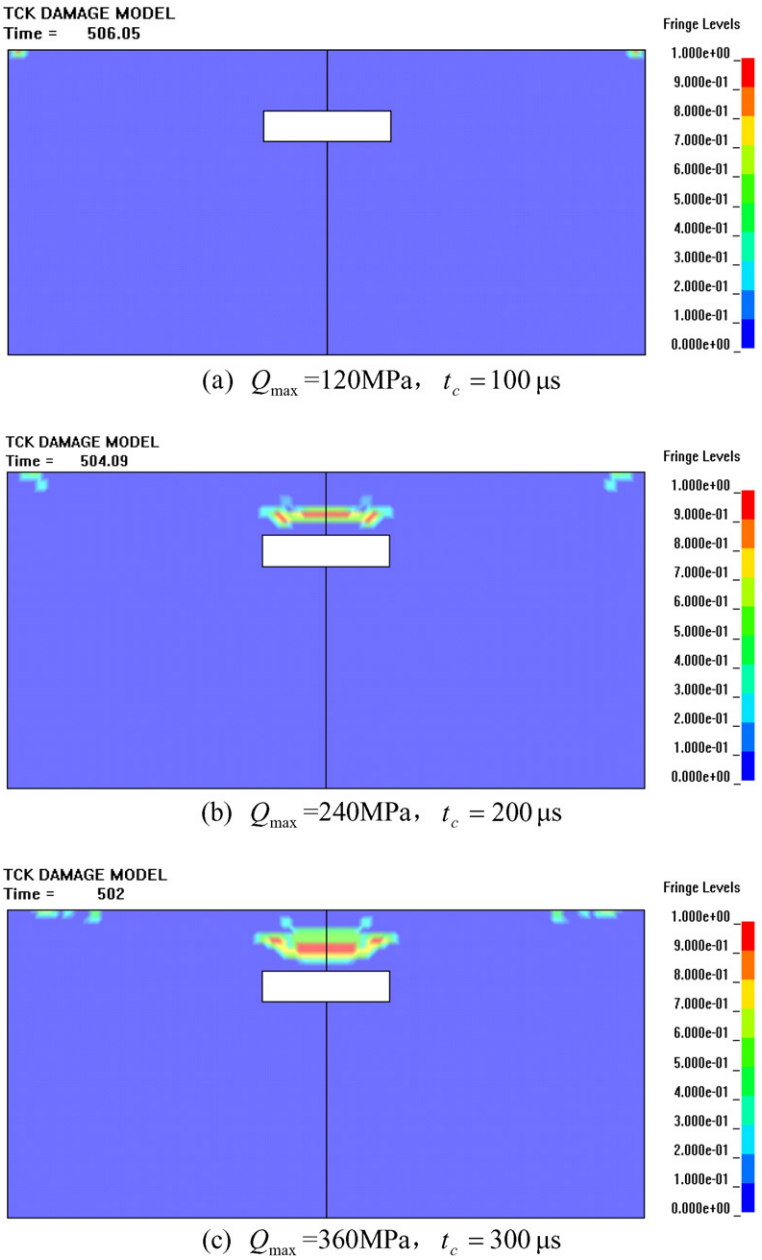

Fig. 13. Development of tensile damage with blast loading ($l = 0.60$ m, $h = 0.30$ m and $e = 0.60$ m) at $t = 500$ μs.

sile waves become stronger under the higher external loadings.

4.3.2. Effect of cavity width h

Four values of $h = 0.30$, 0.60, 0.90, 1.20 m, when $l = e = 0.30$ m, are considered to study the effect of cavity width on the attenuation of stress-waves. The numerical results are shown in Fig. 14. It is noted that the cavity width h has little influence on the decay factor for the peak P.

4.3.3. Effect of cavity position e

The effect of cavity position e is examined here. The e values are taken as 0.30, 0.60, 0.90 and 1.20 m when $l = h = 0.30$ m. Fig. 15 compares the curves of P versus t. For all e values, the peak values

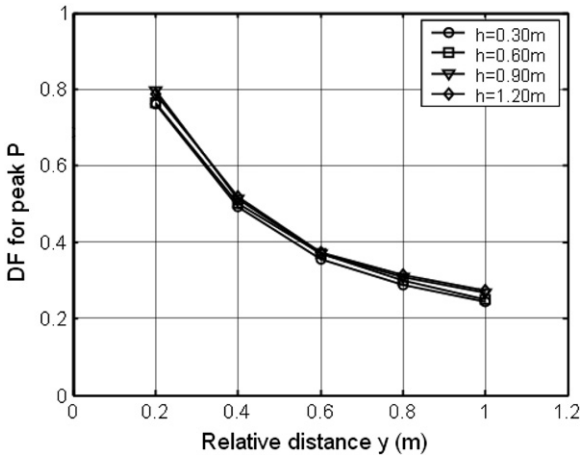

Fig. 14. Variation of decay factors for peak P with different widths h of cavity.

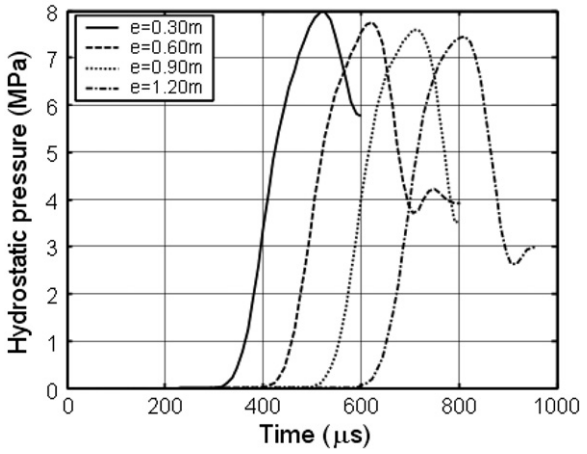

Fig. 15. Effect of cavity position e on hydrostatic pressure history at $y = 0.5$ m point on Y-axis.

do not vary much, but the arrival time of the peak values gradually lags with an increase of the propagation distance of stress-waves. Fig. 16 shows the decay factor of the peak σ_y versus relative distance y. It is evident that all the curves are almost identical. Therefore, the position e of the cavity has little influence on the decay factor for the peak σ_y.

4.3.4. Empirical formula for decay factor

Based on the above numerical results, the effects of h and e on the peak P are established to be insignificant. Thus, DF can be considered as a function of length l and relative distance y:

$$DF = f(y, l) \tag{14}$$

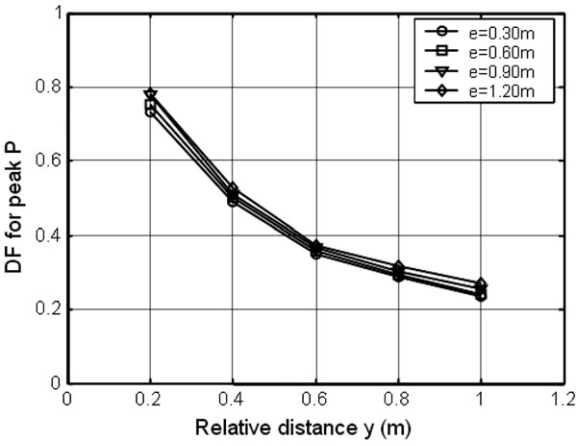

Fig. 16. Variation of decay factors for peak P with different positions e of cavity.

In order to determine the particular form of Eq. (14), one value of e (0.30 m), four values of l (0.30, 0.60, 0.90 and 1.20 m) and five values of y (0.2, 0.4, 0.6, 0.8 and 1.0 m) are chosen from Fig. 11. Through a curve fitting regression analysis, the DF for the peak P at a specified point on the Y-axis is approximately expressed as follows:

$$\mathrm{DF} = \exp\left(-\frac{y}{2l}\right) \tag{15}$$

This formula shows that DF increases with l and decreases with y. When term $\frac{y}{l}$ approaches zero, DF is almost equal to unity. Fig. 17 shows a comparison between the numerical results and the predictions from the empirical formula. Good agreement can be observed. Therefore, Eq. (15) can be used to estimate the length l of a rectangular cavity if the

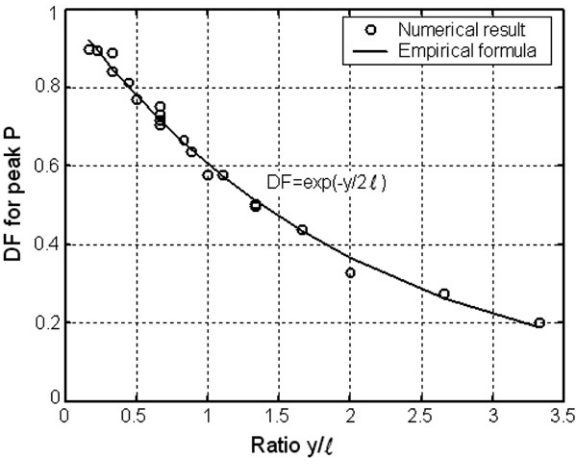

Fig. 17. Comparison of empirical formulae and numerical results of decay factors for peak P.

expected DF at a relative distance y is given. When DF and l are given, Eq. (15) can also be used to estimate the nearest safe distance (i.e. $y_{\min}$).

5. Conclusions

Continuous demands on safety and intelligent design have placed increasing emphasis on performance analyses of concrete defense structures. This paper consists of three aspects: user-defined constitutive subroutine, numerical investigations and empirical formula. From these studies, the following conclusions and understandings may be drawn.

(1) The TCK model is realized by coding it as user subroutine in the dynamic finite element program LS-DYNA. It not only can capture the tensile damage above cavities or near non-transmission boundaries but also can evaluate the elastoplastic behaviors of concrete in compression.
(2) Artificial cavities embedded in the concrete defense layer exert significant influences on the attenuation of stress-waves. For a rectangular cavity, the decay factor largely depends on its length, while its width has little effect if the width is larger than 0.30 m in our computations.
(3) One empirical formula is obtained to correlate the decay factor for peak P, dimensions of a cavity and relative distance. The formula can be employed to determine the minimum length of a cavity $l_{\min}$, or minimum safe distance $y_{\min}$ when the decay factor is given. Therefore, it can serve as useful tools in the design of intelligent defense engineering.

Acknowledgements

This work reported herein was partially supported by the Postdoctoral Science Foundation of China (Project no.2004036468). The authors also wish to express their gratitude to *The Third Institute of the Corps of Engineers* for providing materials of filed experiments.

References

[1] R.P. Kenedey, A review of procedure for the analysis and design of concrete structure to resisting missile impact effects, Nuclear Engineering 37 (1976) 183–203.
[2] D.V. Balandin, N.N. Bolotnik, W.D. Pilkey, Optimal Protection from Impact, Shock, and Vibration, Gordon and Breach Science Publisher, Toronto, 2001.
[3] T.L. Teng, Y.A. Chu, F.A. Chang, H.S. Chin, Numerical analysis of oblique impact on reinforced concrete, Cement & Concrete Composites 27 (2005) 481–492.
[4] T. Krauthammer, Blast-resistant structural concrete and steel connections, International Journal of Impact Engineering 22 (1999) 887–910.
[5] T.P. Philippidis, T.G. Aggelis, Experimental study of wave dispersion and attenuation in concrete, Ultrasonics 43 (2005) 584–595.
[6] Z.L. Wang, Y.C. Li, J.G. Wang, Study of stress waves in geomedia and effect of a soil cover layer on wave attenuation using a 1D finite difference method, Computers and Geosciences 32 (2006) 1535–1543.
[7] Y.C. Li, X.J. Wang, X.Z. Hu, Study on layered design and its defending function, Technical Report of National Defense Engineering, USTC, China, 2004.
[8] B. Rohani, Shielding methodology for conventional kinetic energy weapons, Technical Report SL-8f-8. U.S. Army engineers Corps, Waterways Experimental Station, Vicksburg. M.S, 1987.
[9] Z.L. Wang, J.G. Wang, Y.C. Li, C.F. Leung, Attenuation effect of artificial cavity on air-blast waves in an intelligent defense layer, Computers and Geotechnics 33 (2006) 132–141.
[10] L.M. Taylor, E.P. Chen, J.S. Kuszmaul, Micro-crack induced damage accumulation in brittle rock under dynamic loading, Computer Methods in Applied Mechanics and Engineering 55 (1986) 301–320.
[11] E.P. Chen, Simulation of concrete perforation based on a continuum damage model, in: A. Carpinteri (Ed.), Size-Scale Effects in the Failure Mechanisms of Materials and Structures, E & FN Spon Press, 1996.
[12] Livemore Software Technology Corporation (LSTC), LS-DYNA Keyword User's manual, California, USA, 2003.
[13] B. Budiansky, R.J. O'Connell, Elastic moduli of a cracked solid, International Journal of Solids and Structures 12 (1976) 81–97.
[14] D.E. Grady, M.E. Kipp, Continuum modelling of explosive fracture in oil shale, International Journal of Rock Mechanics and Mining Sciences 17 (1980) 147–157.
[15] R. Englman, Z. Jaeger, Theoretical aids for the improvement of blasting efficiencies in oil shale and rocks, AP-TR-12/87, Soreq Nuclear Research Center, Yavne, Israe,1987.
[16] E.P. Chen, Non-local effects on dynamic damage accumulation in brittle solids, International Journal for Numerical and Analytical Methods in Geomechanics 23 (1999) 1–21.
[17] D.E. Grady, The mechanics of fracture under high-rate stress loading: In Bazant, Z.P. (Ed.), Preprints of the William Prager Symp. on Mechanics of Geomaterials: Rocks, Concrete and Soils, Northwestern University, Evanston, IL, 1983.
[18] D.R.J. Owen, E. Hinton, Finite elements in plasticity: Theory and Practice, Pineidge Press, Swansea, UK, 1980.
[19] S. Guruprasad, A. Mukherjee, Layered sacrificial claddings under blast loading, Part I – analytical studies, International Journal of Impact Engineering 24 (2000) 957–973.
[20] P.S. Bulson, Explosive loading of engineering structures, E & FN Spon Press, London, 1997.
[21] J.O. Hallquist, LS-DYNA Theoretical Manual, California, USA, 1998.